1 Plasmon Coupling

Both the resonant field enhancement and the confinement of a surface plasmon can be improved by bringing a second surface plasmon into close proximity. Similar to coupled harmonic oscillators and dipoles, plasmons couple together via Coulomb forces, forming normal modes of oscillation. The charge distributions of the resulting normal modes depend sensitively on the particle separation and are strongly confined to the dielectric space between metallic surfaces where charges strongly interact. These normal modes are therefore more generally known as *gap plasmons* and lead to tuneable plasmon resonances [**huang2010**, **millyard2012**] and significant increases in field enhancement, enabling single molecule spectroscopy [**mertens2013**, **taylor2014**].

Coupled plasmons are a feature of many metallic nano-systems with closely spaced metal-dielectric interfaces, including metal-insulator-metal (MIM) and insulator-metal-insulator (IMI) waveguides [**maier2007plasmonics**, **lindquist2013**] and systems containing multiple metallic nanoparticles (MNPs) [**maier2002**, **atay2004**, **muskens2007**, **huang2010**, **millyard2012**, **taylor2011**, **herrmann2013**] or nanoparticles-on-mirror (NPoM) [**okamoto2003**, **daniels2005**, **kinnan2007**, **mubeen2012**, **mertens2013**, **denijs2014**]. For the purposes of this work, discussion is restricted to the ideal case of coupled localised surface plasmons (LSPs) between two closely spaced MNPs, closely representing the experimental system, though the description of coupling is valid for many other cases involving SPs. Furthermore, in each example of coupled systems, the physics can be reduced to interactions between neighbouring charge distributions. Understanding the simple dimer system is therefore important to fully understand more complex geometries.

In the simplest description, the Coulomb interaction between free electrons in adjacent MNPs introduces an additional coupling force, pulling charge towards the gap between metallic surfaces. A greater amount of charge accumulates on the gap-facing metallic surfaces. As particles move closer together this force grows, more strongly confining the charge and increasingly polarising the gap region. The resonance frequency of the individual plasmon mode shifts from ω_0 by $\Delta\omega$ depending on the strength of coupling. The sign of $\Delta\omega$ depends on whether coupling is attractive or repulsive. Similar to coupled oscillators, the two coupling configurations (normal modes) along each axis are the in-phase bonding and anti-phase anti-bonding modes. Light generally drives the free electrons of two sub-wavelength particles in phase, resulting in only an observable bonding configuration. Plasmons excited along the dimer axis experience an attractive coupling force in the bonding configuration, redshifting with decreasing interparticle separation, whereas plasmons excited perpendicular to the dimer axis experience repulsive coupling in the bonding configuration, blueshifting with decreasing interparticle separation. Compelling evidence for each of these modes has been seen many times, with particularly good results found using chains of AuNPs [**maier2002**],

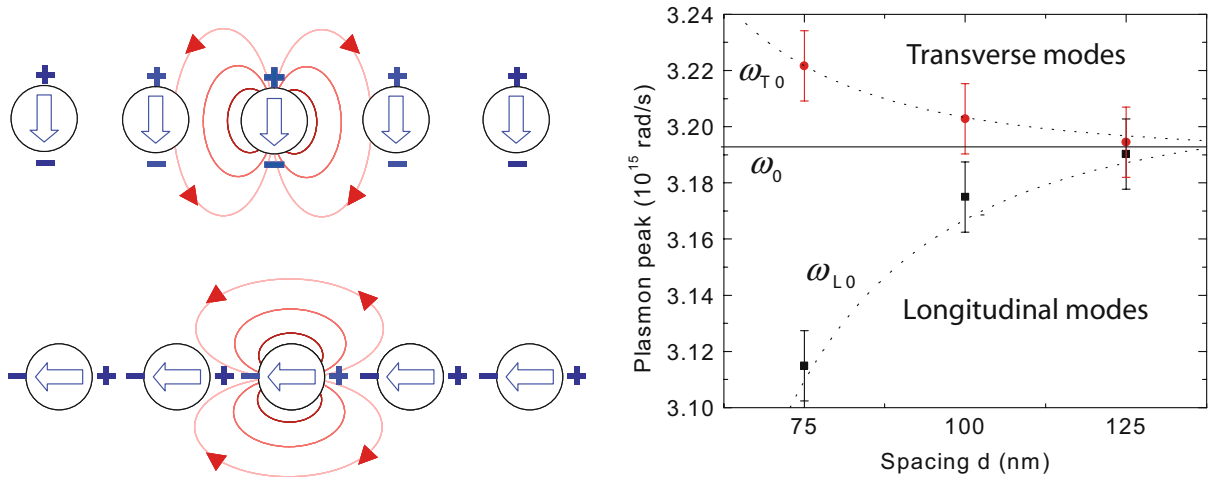

Figure 1: Experimental and theoretical plasmon coupling. Dipolar plasmons in chains of spherical AuNPs couple depending on field orientation [**maier2007plasmonics**] (left). Experimentally measured plasmon resonance energies in coupled AuNP chains show the gap-dependent tuning due to coupling [**maier2002**] (right). The dotted line corresponds to a r^{-3} point dipole model.

as shown in Figure 1. In almost all cases, it is the bonding plasmons oriented along the dimer axis that are of interest.

The primary effect of plasmon coupling orientated across the dimer gap is increased confinement of the electric field to the dielectric gap medium, leading to much larger field enhancements that can be exploited for sensing. For a strongly confined gap mode there is very little field in the metal with almost all field confined within a small lateral mode within the gap [**romero2006**]. This is known as a plasmonic "hot spot". Through this mechanism alone the field enhancement $|E/E_0|$ can be increased by more than an order of magnitude [**hao2004**, **talley2005**]. Hence, in recent years, the interests of the plasmonics community have shifted from individual plasmonic nanostructures to coupled systems in order to maximise nano-optical performance. This has led to the progression into sub-nm plasmonic cavities, the study of which is a focus of this project. The development of a theoretical model for such small systems begins with the classical models of plasmon coupling with additional complexity added until quantum mechanical effects become apparent.

1.1 Classical Models of Plasmonic Coupling

Two analytical classical models exist to describe plasmon coupling. The first and simplest model continues the description of the dipole plasmon present in small (quasistatic) MNPs and introduces dipole-dipole interactions. The second model of plasmon hybridisation is more complex and successfully models higher order modes of charge oscillation.

1.1.1 Dipole-Dipole Model

In its simplest case, interactions between dipolar plasmons in small MNPs appear similar to dipole-dipole interactions [**kreibig1995optical**, **maier2002**, **gluodenis2002**, **rechberger2003**, **atay2004**], exhibiting the same behavioural dependence on separation and relative orientation with respect to the incident field. Examples of some commonly considered dipole-dipole interaction geometries are shown in Figure 2. In each situation the electric field incident on a dipole $\mathbf{p}_1$ is perturbed by the presence of a second dipole $\mathbf{p}_2$ a distance r away, whose fields as given in Eq. **??** are superimposed onto the incident field at the location of $\mathbf{p}_1$. The result is in an effective field given by,

$$\mathbf{E}_{\parallel}(\mathbf{p}_1) = \mathbf{E}_{0,\parallel} + \frac{\mathbf{p}_2}{2\pi\varepsilon_0\varepsilon_d r^3}, \tag{1a}$$

$$\mathbf{E}_{\perp}(\mathbf{p}_1) = \mathbf{E}_{0,\perp} - \frac{\mathbf{p}_2}{4\pi\varepsilon_0\varepsilon_d r^3}, \tag{1b}$$

where $\parallel$ and $\perp$ denote the orientation of dipoles relative to the dimer axis. The sign of the second term in each equation determines the effect of coupling whilst its strength falls as r^{-3} due to $V \propto p_1 p_2 r^{-3}$ [**halas2011**]. The polarisability of the MNP is modified by this additional interaction field, changing the frequency at which it becomes resonant. For two dipoles aligned end-to-end ($p \parallel r$) and driven in phase, coupling is attractive (increased **E**, Eq. 1a), leading to a decrease (redshift) of the resonant frequency. Conversely, the interaction between two dipoles aligned side-by-side ($p \perp r$) is repulsive (decreased E, Eq. 1b), causing an increase (blueshift) of the resonant

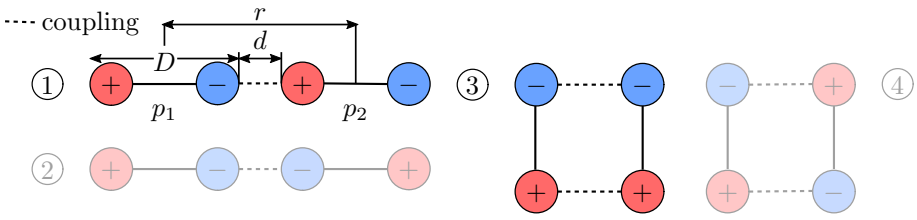

Figure 2: Diagram of dipole interactions. The distance between dipoles of length D is r with an edge-to-edge separation d. Configurations 1 and 3 are comparable with plasmon coupling as a result of sub-wavelength structures being driven by a single external light field. Configurations 2 and 4 are generally unphysical or non-radiative in plasmon dimers without asymmetry or phase retardation.

frequency. These describe the in-phase interactions between two dipole. Anti-phase configurations, as shown in Figure 2, behave in the opposite manner to the in-phase counterparts as the direction of the Coulomb force reverses. These configurations are often ignored in quasistatic dimers since light only drives in-phase oscillations. Electron-based techniques such as EELS are instead used to probe these 'dark' modes. Using EELS with AuNP chains, the validity of the dipole approximation was confirmed, showing good agreement with the experimental data shown in Figure 1 [**maier2002**].

The dipole-dipole model is only an approximation to actual plasmonic coupling and does not adequately account for the spatial charge distribution. It can be somewhat improved by taking into account the finite particle size. Since the internal restoring force within particles, scaling as D^3, contributes to the potential, the interaction energy goes as $(r/D)^{-3}$ as opposed to r^{-3} [**jain2007**]. Furthermore, this quantity is redefined to better represent a dimer using the gap width, d, as $(d/D) = (r/D) - 1$. The resonant wavelength shift due to attractive coupling can then be approximated using a "plasmon ruler" equation [**jain2007**, **ben2011**],[1]

$$\frac{\Delta\lambda}{\lambda_0} = a \exp\left[-\frac{(d/D)}{\tau}\right], \tag{2}$$

where a is the coupling strength and τ is a decay constant. In essence, this model describes an interesting phenomenon - that plasmon coupling is scale invariant. Dimers comprised of larger particles interact more strongly for the same separation than smaller dimers. However, their relative shifts depend on how the gap size compares with the particle size. In recent years this relation still shows good agreement with experimental data but the approach remains limited to describing only dipolar modes in simple geometries [**muskens2007**].

1.1.2 Plasmon Hybridisation

A slightly more complex model, known as plasmon hybridisation, was developed to more generally explain the formation and behaviour of coupled modes [**prodan2003**, **prodan2004**, **nordlander2004**]. In this model, plasmon

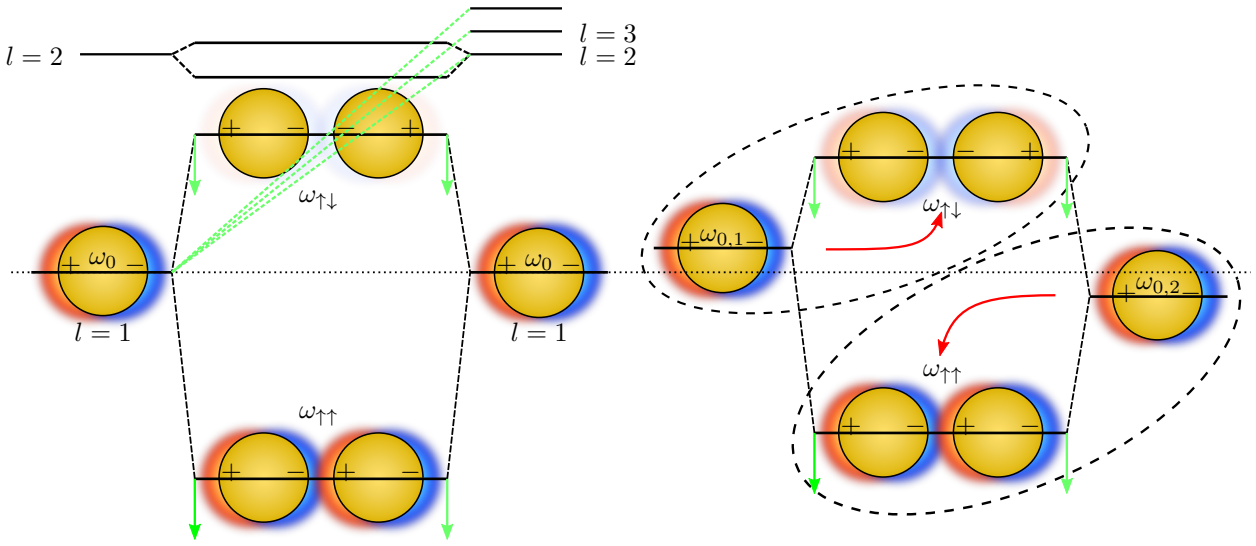

Figure 3: Diagram of plasmon hybridisation between coupled plasmons in a nanoparticle dimer. Plasmons are coupled along the dimer axis. Coupling leads to bonding and anti-bonding modes for each set of interacting l modes (left). Interaction with higher order l modes lowers the overall energy of lower order coupled modes (green lines). Only the bonding ($\omega_{\uparrow\uparrow}$) mode in the symmetric (homo-)dimer has a net dipole moment and is therefore observable. Cancellation of the net dipole moment means the anti-bonding ($\omega_{\uparrow\downarrow}$) mode remains optically dark. On the contrary, asymmetry in a (hetero-)dimer means both modes stay bright (right). In this case, the lower and higher energy individual modes shift to form the bonding and anti-bonding hybridised modes, respectively. This diagram is adapted from [**nordlander2004**].

[1] The exponential approximates a more complex power law [**kadkhodazadeh2014scaling**].

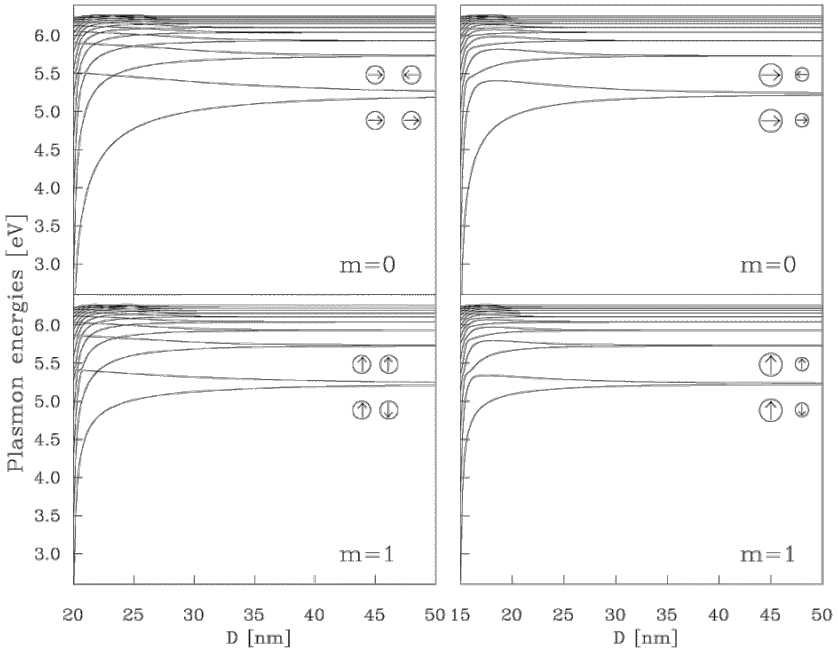

Figure 4: Hybridised plasmon energy shifts for spherical AuNP dimers. Homodimer (left) and heterodimer (right) plasmon energies are calculated in both the axial (top) and transverse (bottom) coupling configurations. Spheres are 10 nm in diameter in the homodimer and 10 nm and 5 nm in the heterodimer.

resonances are mechanically modelled as resonant oscillations of an incompressible fluid confined within an equilibrium geometry [**prodan2004**]. The plasmon resonances of a more complex particle geometry are then solved by decomposing it into coupled resonances of two simpler particle geometries [**prodan2003**, **prodan2004**]. This is done in analogy with the ideas underpinning molecular orbital hybridisation and the hybridisation of quantum energy states. Using this logic, the theory equally describes the plasmon resonances of two coupled simple particle geometries [**nordlander2004**] or a particle coupled with its image charge in a surface [**nordlander2004a**]. Under these circumstances, the multipolar modes of each of the individual dimer particles energetically split into two hybridised modes representing the bonding (in-phase) and anti-bonding (anti-phase) configurations. This behaviour is shown in Figure 3.

Unlike the dipole-dipole model, plasmon hybridisation is capable of predicting higher order multipolar modes in a coupled dimer system as well as dealing with more complex geometries. It is therefore valid for describing larger dimer geometries and smaller gap sizes. As with dipole-dipole interactions, the bonding and anti-bonding hybridised modes redshift and blueshift from their initial mode positions upon decreasing the separation, respectively. These shifts in the plasmon energies are shown in Figure 4. However, the addition of higher order modes to the classical description of plasmon coupling, and their interaction with adjacent modes of similar energies, modifies the rates of each mode's shift, as shown by the green lines in Figure 3 [**nordlander2004**]. These interactions leads to a further redshift of each affected mode, though only in the case of small gaps or larger particles when higher order modes are excited.

In each classical approach it is the resulting dipole moment of each coupled mode that dictates its radiative properties. The in-phase bonding mode exhibits a large dipole moment and strongly couples with light whereas the anti-phase anti-bonding mode has no net dipole moment in a symmetric, quasistatic system and thus remains dark. This remains the case until the anti-bonding dimer mode acquires a finite net dipole moment, either through particle asymmetry (difference material, size or shape) or phase retardation across the dimer (large particles, non-quasistatic)[2], at which point it becomes more radiative and hence experimentally observable using optical methods. Alternatively, local excitation of specific charge distributions using EELS allows for measurement of dark modes [**chu2008**, **koh2009**]. Should both bonding and anti-bonding modes be bright and gaps decrease

[2]Phase retardation of the driving field across the dimer breaks the coupling symmetry, allowing anti-phase modes to be excited.

enough that a blueshifting anti-bonding mode approaches on a higher order redshifting bonding mode, an anti-crossing will occur and modes exchange symmetry. This causes anti-bonding modes to eventually redshift into geometrical contact.

Whilst each of the previously described analytical models has found some success in describing experimentally observed plasmon coupling in simple systems, their approaches are limited in scope. Neither model directly calculates electrodynamics and solves the actual electromagnetic problem. Instead, they use analogies to similar electromechanical systems to provide a useful insight into the mechanism of plasmon coupling. The electrodynamics of a particular plasmonic problem are now often solved using computationally demanding, numerical techniques, in which the electrodynamics are solved at each boundary within a system.

1.2 The Dynamical Optical Response of Plasmonic Dimers: Transitioning from Capacitive to Conductive Plasmonic Coupling

Using modern numerical simulation techniques, such as the boundary element method (BEM) and finite-difference time-domain (FDTD) approaches, the full separation-dependent optical response of a plasmonic dimer has been calculated as particles transition from non-interacting to coupled through into geometrical contact [**romero2006**]. In these calculations, the lowest order plasmons hybridise, redshift and more intensely scatter as the separation decreases, with higher order modes eventually emerging. Classically, this leads to a large number of modes being present in nanometre-size gaps. The lateral confinement of the field between particles of radius R separated by a gap of width d is estimated as $w = \sqrt{Rd}$ [**romero2006**]. As higher order modes become more intense, scattering from lower order modes decreases. Despite this, their field enhancement continues to rise [**esteban2012**]. These plasmons become so confined that they no longer couple with the far-field. This behaviour continues until particles are nearly touching into geometrical contact.

Once touching, bonding hybridised plasmons abruptly transition into charge transfer plasmons (CTPs) - charge oscillations spread across the full extent of the connected dimer. These are widely observed in geometrically contacted or overlapping plasmonic systems [**atay2004**, **lassiter2008**]. A dipolar CTP emerges at lower energies (considered to be the equivalent of a monopolar dimer mode) as screened hybridised plasmons are expelled out of the gap, transitioning into higher order CTPs due to their similar charge distributions [**romero2006**, **perez2010**, **perez2011**, **tserkezis2014**]. Their resonances blueshift, diminishing in intensity and broadening in width as a result of significantly increased currents. The lower energies of CTPs are associated with a spatially larger dipole, as shown in Figure 5, suggesting they should blueshift with increasing particle overlap. Their broad width compared with capacitively coupled plasmons is caused by dissipation in the junction and can be linked with behaviour described by Eq. **??**.[3]

Classical predictions of plasmon coupling break down at small, sub-nm gaps where the continuum of excited higher order modes redshift to a singularity as $d \to 0$, and the field enhancement increases infinitely. This be-

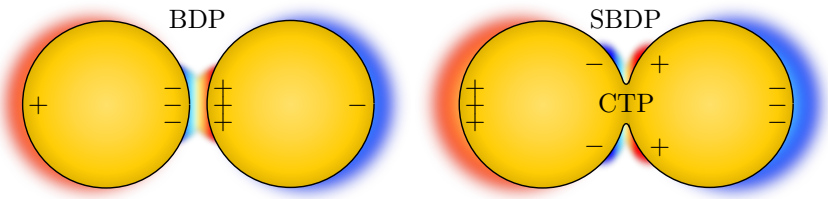

Figure 5: Diagram showing the emergence of charge transfer and screened bonding (crevice) plasmons on geometrical contact in a nanoparticle dimer. The field generated by the bonding dimer plasmon (BDP) is screened from the gap by the conductive contact, forcing capacitive coupling to the crevice gap in the form of the screened bonding dimer plasmon (SBDP). The dominant charge oscillation is then the charge transfer plasmon (CTP) through the conductive bridge and across the whole structure.

[3]For a spherical MNP dimer with a bonding hybridised dipolar plasmon (BDP) and bonding hybridised quadrupolar plasmon (BQP) the corresponding CTP modes are typically labelled as the CTP and CTP′. The CTP′ is often labelled as the screened bonding dipolar plasmon (SBDP) due to the similarities in the charge distributions between a second order CTP and first order bonding mode.

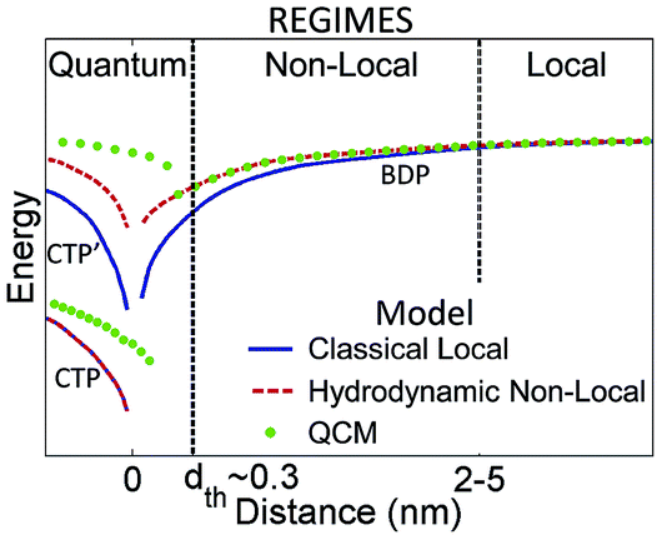

Figure 6: Calculated plasmon energies of a spherical AuNP dimer as a function of gap separation using a number of computational models [esteban2015]. The classical local approach is valid for separations greater than 2 nm. Below this non-locality smooths the gap and adequately describes mode behaviour until 3 Å. At this point quantum models must be used. Figure taken from [**esteban2015**].

haviour is completely unphysical and is rectified once non-locality and quantum mechanical effects are considered. A comparison of the models taking these effects into account is shown in Figure 6. Quantum mechanical effects begin to affect plasmon coupling under two conditions - either the particles become sufficiently small that quantum non-locality and non-local effects (finite, non-negligible electron wavefunction spill-out from the particle) become important or the gap size decreases to scales on which quantum tunnelling and non-locality of the gap surfaces can no longer be ignored.

Non-locality, the spill-out of electrons from the surface of the metal, smooths the gap geometry, and consequently the spectral trends. The redshift into contact is heavily reduced compared with classical predictions. Smoothing of the sharp edges in the gap rectifies the continuum of higher order modes, which are then harder to excite, leaving only the most fundamental dimer modes. Redshifts are reduced since electrons move further into the metal on approach, suppressing coupling [**esteban2015**]. The emergence of CTPs and screening of the bonding hybridised modes prior to geometrical contact are predicted only once quantum charge transfer effects are accounted for. The onset of quantum tunnelling means charge is transported across the gap without requiring geometrical contact, neutralising some of the accumulated plasmon charge. Tunnelling is then followed by ballistic change transport prior to returning to a classical description of plasmonics. These two effects, due to their significance in dimer systems, are considered in more detail.

1.2.1 Quantum Charge Transport: Electron Tunnelling and Ballistic Transport

The quantum charge transport properties of a system consisting of two reservoirs of free electrons separated by a potential barrier are determined by how the height of the potential barrier compares with the Fermi energy of each reservoir. For two metals separated by an insulating gap the potential barrier will be larger than the Fermi level. Classically, electrons with energies below the potential barrier cannot reach the other side. Electrons can only conduct through via quantum tunnelling, in which electrons incident on thin barriers have a finite probability of passing directly through the barrier as opposed to going over it. This is shown in Figure 7.

The potential barriers and transmission probabilities of a tunnel junction between two reservoirs of Au are shown in Figure 8. In a simplistic model, the potential layout is considered as a 1D rectangular barrier and the tunnelling probability increases exponentially with decreasing barrier width, d, going as $T = \mathrm{e}^{-\beta d}$, where β is

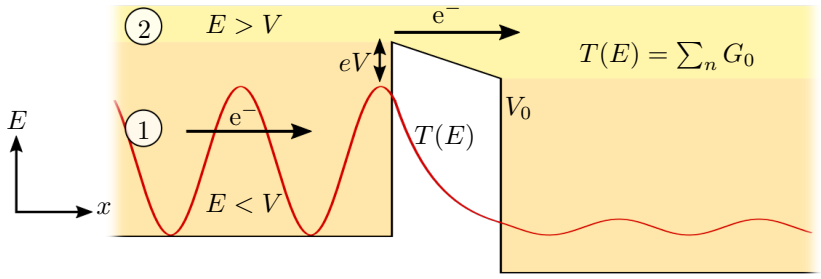

Figure 7: Diagram of quantum charge transport between two reservoirs of free electrons. If the Fermi energy of electrons is below the barrier potential (1) then there is a finite transmission probability $T(E_F)$ of tunnelling through the barrier. If the Fermi energy becomes larger than the potential barrier electrons are free to move through a number of quantised conductance channels of conductance $2e^2/h$.

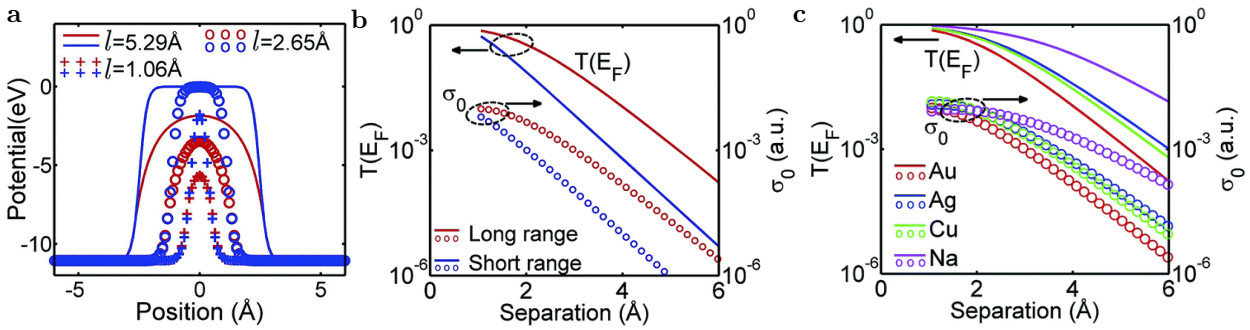

Figure 8: Potential barrier shapes for various gap widths and tunnelling transmission probabilities as a function of separation and material [esteban2015]. Calculated potential barrier shapes between two Au particles as a function of separation (a) with corresponding transmissions (b). The inclusion of long-range image charge interactions is compared with a simple short-range barrier model. Realistic barrier shapes are more rounded than the simpler rectangular assumption. Overlap between rounded potential edges decreases the barrier height with reduced separation. Tunnelling increases exponentially as the gap width reduces, with increased tunnelling caused by the smaller rounded barriers. Transmission depends on the work function of a material with differing transmission probabilities at a given separation (c).

a decay parameter [**griffiths2005introduction**].[4] Many different mathematical descriptions of this phenomena exist [**simmons1963generalized**, **blanco2006stm**], especially after the invention of STM, that predict the conductance and resulting current density as electrons tunnel through an arbitrary potential landscape. This is in part due to the large number of parameters that influence tunnelling (e.g. work function, barrier potential, barrier shape, applied bias, temperature, charge hopping [**blanco2006stm**]) and the extension of it into 3D gap morphologies, however the exponential decay is always present.[5] The current density is therefore expected to follow [**tan2014**],

$$J = J_0 \mathrm{e}^{-\beta d}, \tag{3}$$

where J_0 is a saturation current density. This behaviour holds for large gap sizes but begins to fail in small (2 Å) gaps where the rectangular barrier shape assumption no longer holds (Figure 8a,b). The barrier height begins to decrease with separation on overlap of the rounded edges. Tunnelling then becomes even more likely as the separation decreases. Since the transmission depends on the Fermi energy of free electrons in a material and the potential of the barrier region in between, different materials have different tunnelling responses. For example, tunnelling is far stronger in Na than in Au (Figure 8c) [**esteban2015**]. Finally, the current generated by

[4] For a simple rectangular barrier of height V_0 the transmission $T = |t|^2$ is given by, $T = \mathrm{e}^{-2\sqrt{\frac{2m}{\hbar^2}(V_0 - E)}d}$.
[5] At least within a low bias approximation, which is generally valid in the context of this thesis.

tunnelling depends on the number of tunnelling channels available in a junction and the transmission coefficient of each channel [**zuloaga2009**].

Once the barrier falls below the Fermi level (at ∼1–2 Å), provided that the contact is short enough that motion is ballistic (no scattering), conduction electrons can move freely between the two reservoirs via a number of discretely quantised, 1D conduction channels under the application of an applied bias. This bias in the plasmonics case stems from the field induced by light. Each channel has a transmission probability $T(E_F) = 1$ and a conductance given by $\mathrm{G}_0 = 2e^2/h$, the conductance quantum [**landauer1957spatial**]. The total conductance depends only on the number of open channels, a quantity depending typically on the width of the conductive region or the atomic scale contacts between reservoirs. This results in a conductance described by the Landauer formula[6] [**landauer1957spatial**],

$$G = \frac{2e^2}{h} \sum_n T_n(E_F) = n\mathrm{G}_0, \tag{4}$$

where n is the number of transmission channels. Though still firmly in a quantum domain, ballistic transport is a form of conductive contact as opposed to a tunnelling phenomenon. Classical behaviour is only recovered if the length of the constriction increases to the point at which electrons begin to scatter or the width increases to allow many channels. In this event, the conductance is classified as diffusive with a conductance given by $G = \sigma A/d$.

1.2.2 Quantum Charge Transport in Plasmonic Nanogaps

The effects of quantum charge transport were first predicted in small ($R < 2\,\mathrm{nm}$) NaNPs using full quantum mechanical, time-dependent (TD) density functional theory (DFT) calculations [**zuloaga2009**]. Since these calculations consider the behaviour of each electron, they are currently limited in complexity to small systems containing less than 2000 electrons. Quantum effects in larger metallic nanostructures are predicted by the quantum corrected model (QCM), a classical model which includes the effects of non-locality and uses an effective gap dielectric function that takes into account the conductivity induced by quantum effects using pre-calculated values from TDDFT [**esteban2012**]. Both the QCM and TDDFT show agreement on the effects of tunnelling and conduction on plasmon coupling in NaNPs, with QCM predictions of the plasmon energies in a AuNP dimer shown in Figure 6. Experimentally, evidence of quantum transport effects in plasmonic gaps has recently been found using optical spectroscopy [**savage2012**, **cha2014**, **zhu2014**], EELS [**scholl2013**], SERS [**zhu2014**], photoluminescence [**kravtsov2014**] and third-harmonic generation measurements [**hajisalem2014**].

In numerical simulations, the onset of tunnelling creates a conductive bridge through which electrons can transmit during each half optical cycle. Charge transfer across the junction neutralises some of the accumulated plasmon charge on gap surfaces, lessening the local capacitive interaction. This is the screening effect. Electron tunnelling increasingly screens coupling leading to a reduction in the rate of redshift. The appearance of this additional contribution to coupling signifies entry into the *crossover* regime [**zuloaga2009**]. At these separations, typically 5 Å in Na, the barrier remains above the Fermi level. The most prominent effect of screening is a drastic decrease of the field enhancement in the gap as bonding hybridised modes are gradually expelled from the gap [**zuloaga2009**, **esteban2012**]. In theory, this prevents small gaps from being useful as SERS structures but instead provides a method for optically studying electron transport on sub-nm length scales, motivating the need to fully understand these effects.

The conductance provided by gap sizes characteristic of tunnelling is too small to excite CTPs, hence only screening is initially observed. Once the gap size reduces to the point at which the barrier falls below the Fermi level a dimer transitions into a conductive state where $T(E_F) = 1$ and conductances are given by Eq. 4. This is the *conductive* or *CTP* regime. A diagram showing the changeover in conduction mechanisms is shown in Figure 9, similar to the DFT calculations presented in [**zuloaga2009**]. In recent quantum simulations this critical gap width is found between 1–2 Å. A similar drop in barrier heights below the work function of Au is found in Figure 8a between 2.65 Å and 1.06 Å. The free flow of electrons permits a large amount of current through the junction and enables CTP excitation [**zuloaga2009**]. The current immediately increases screening so much that bonding hybridised plasmons decouple and undergo a blueshifting transformation into CTPs. In initial quantum calculations [**zuloaga2009**] the fundamental CTP is not shown but is found in later TDDFT calculations appearing near to geometrical contact once the conductance rises sufficiently [**esteban2012**, **scholl2013**].

[6] Full derivation of the Landauer equation and quantised conductance is found in the appendices.

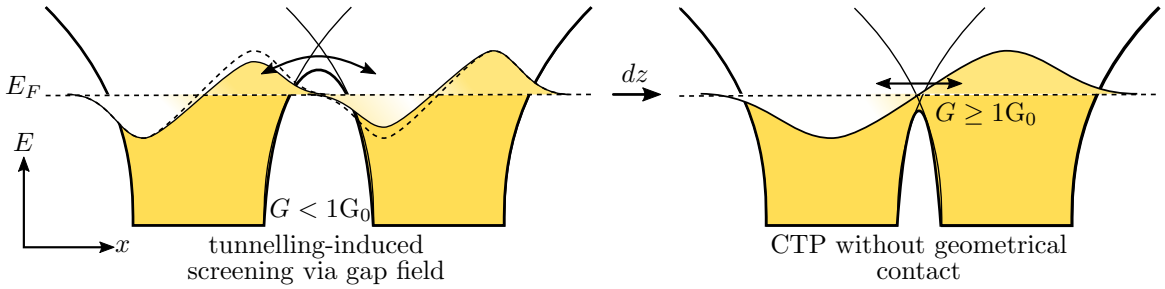

Figure 9: Diagram of the charge transfer process in a nanoparticle dimer. The electron density is represented by the filling of the particle potential wells. Electrons are considered non-local and spill out from the gap surfaces. Long-range image charge interactions also further round the potential barrier. Tunnelling at large distances neutralises optically-driven charge accumulation on gap surfaces, reducing coupling. At smaller separations the particle Fermi level can become greater than the gap potential barrier, permitting conduction instead of tunnelling. This is the origin of gap current and CTP excitation.

Though initial simulations considered only small NaNPs it is proposed that in larger nanoparticle dimers the boundary to the quantum regime would be extended to larger separations as larger nanoparticles have more closely spaced energy levels (reduced quantum size effects) and therefore more available conductance channels [**zuloaga2009**]. In essence, this means that the conductance required to cause these effects remains the same but is achieved through the cumulative contribution of many individual conduction channels. The QCM seemingly reproduces this effect with CTP excitation and blueshifts occurring in $R = 25\,\mathrm{nm}$ Au particles at around the same 2–3 Å separation as in $R = 2.17\,\mathrm{nm}$ Na particles, despite the lower rate of tunnelling between Au surfaces. This indicates that a larger surface generates the same tunnelling conductance as a smaller, more conducting junction, which is enough to produce the same amount of charge transfer in one optical cycle.

A simple estimation of this critical distance is given in [**savage2012**]. The conductive regime is said to dominate once the charge stored in a plasmon becomes less than the charge involved in charge transfer, i.e. the fraction of conductive charge is greater than 50%. The tunnelling conductivity in a rectangular barrier model is,

$$\sigma(d) = \frac{3k_e e^2}{4\pi h} e^{-2k_e d}, \tag{5}$$

where $k_e = \sqrt{2m\varphi}/\hbar$ is the electron wavenumber at the work function, φ. The distance at which this leads to a majority of charge transfer is calculated as,

$$d_{QR} = \frac{1}{2k_e} \ln\left[\frac{3k_e \lambda \alpha}{2\pi}\right], \tag{6}$$

where λ is the wavelength of the plasmon and $\alpha = 1/137$, the fine structure constant. Evaluating this for Au ($\varphi = 4.8\,\mathrm{eV}$) at an 850 nm plasmon wavelength yields a critical separation of 1.6 Å. If instead the larger conductivity from DFT is used, the equation predicts a critical gap size of 3.1 Å, the same value as is shown in QCM spectra. This is the point at which plasmons change from being majority capacitively coupled to majority conductively coupled.

Preliminary experimental measurements of the optical scattering from a dynamic spherically-tipped Au AFM probe dimer clearly show the aforementioned effects. Two coupled plasmon resonances, denoted A and B, begin to weaken during the final 7 Å of the approach into contact (Figure 10a) [**savage2012**]. Distances are determined by comparing with QCM spectra. Modes A and B blueshift upon decreasing past a critical separation of 3 Å and begin to regain intensity. A mode, C, strengthens going into contact. These are the signatures of bonding hybridised modes transforming into CTP modes as field is expelled from the gap and conductive channels bridge the gap. Agreement between experimental and theoretical spectra also reaffirms the assumption that the smooth changeover between capacitive and conductive plasmons occurs once charge is split equally between them.

Though experimental tip dimer spectra and QCM spectra have some discrepancies due to the difficulty in simulating such large tip structures, they qualitatively agree. Further agreement with DFT calculations is found in EELS measurements on 10 nm AgNP dimers, brought together under the influence of the electron beam

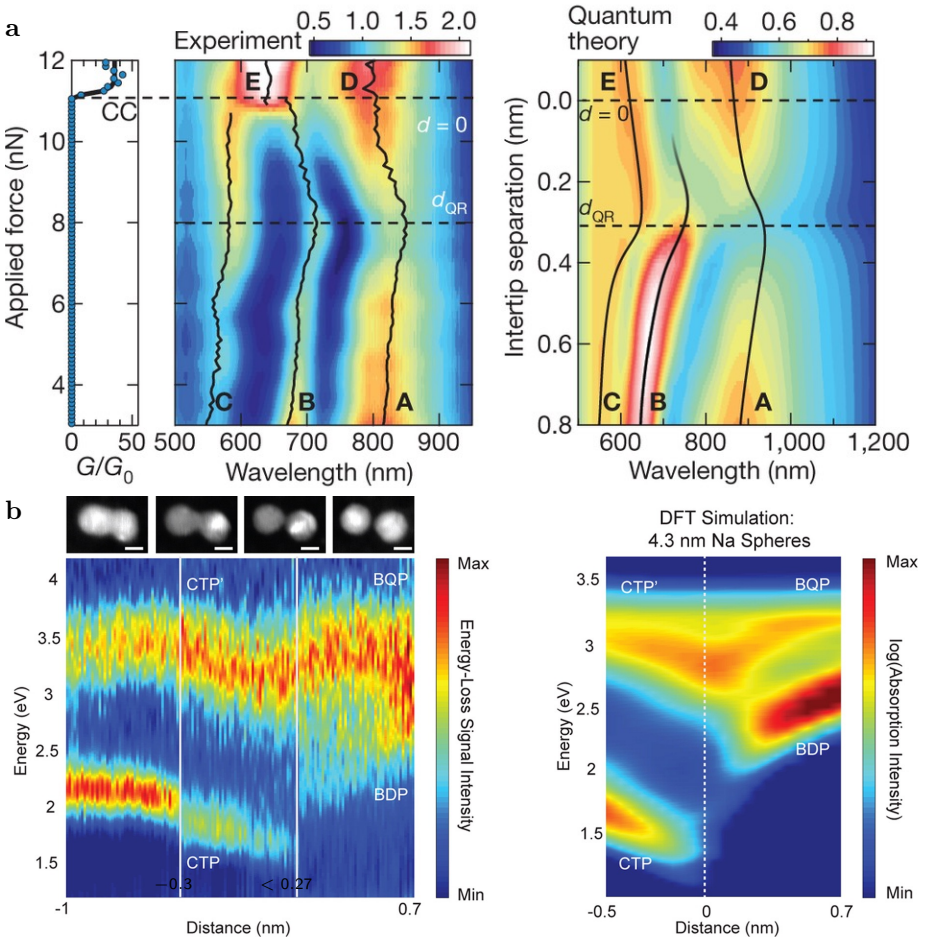

Figure 10: Examples of experimental measurements of the effect of quantum tunnelling on plasmonic gap systems through direct monitoring of the plasmon resonances. (a) Supercontinuum dark-field scattering measurements of two 300 nm diameter spherical Au tips in a dimer configuration with reducing separation, transitioning below 1 nm and into the quantum regime [**savage2012**]. (b) EELS measurements of 10 nm AgNPs being induced closer together by the electron beam [**scholl2013**].

(Figure 10b) [**scholl2013**]. In this system the dimer exhibits screening at 5 Å and the blueshifting transformation between bonding modes and CTPs begins at 3 Å along with the excitation of the fundamental CTP. The agreement between both experiments, the QCM and DFT calculations reinforces the idea that quantum tunnelling screens plasmon coupling and the rising conductance after ballistic conductive contact leads to the rise of CTPs. The observation of a critical distance of 3 Å in many systems of different sizes, shapes and metals is also intriguing and poses further questions of what exactly the conductance is at that point.

A small number of recent experiments have also now began to report effects attributed to conduction and quantum tunnelling. Alkanedithiol molecules of various lengths have been used to discretely tune the gap separation of AuNP dimers, with attenuation and blueshifting of the BDP with molecules smaller than pentanedithiol [**cha2014**]. Similar results are found when using intercalating surface-assembled monolayers (SAMs) [**tan2014**]. Further investigations into sub-nm plasmonic gaps have also shown behaviours attributed to quantum tunnelling, though inferred from properties depending on the field enhancement as opposed to direct measurement of SPRs. A decrease in signal intensity in both the SERS peaks [**zhu2014**] and photoluminescence [**kravtsov2014**] in nano-gap systems, for example, are signatures of quantum tunnelling screening the coupled plasmon field.

A final feature to note about quantum effects is their variability with gap morphology. It has recently been shown theoretically that atomic-scale morphology changes can dramatically alter the plasmonic response through

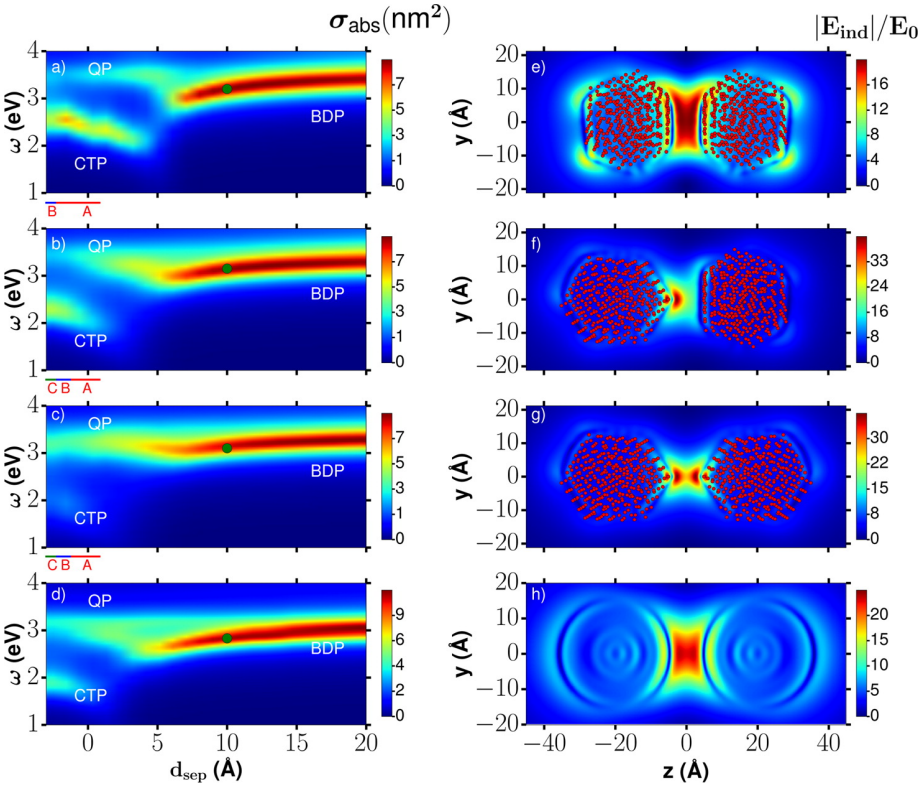

Figure 11: TDDFT calculations of 16 Å faceted NaNP dimers arranged with different facet alignments [barbry2015]. Aligned facets leads to the smallest field enhancement and the earliest onset of charge transfer effects at 5 Å. Vertex alignment results in an atomic-scale lightning rod effect and increased field localisation. CTP excitation is more difficult in this configuration, occurring at 0 Å, due to the small contact but screening is made easier for the same reason, occurring at 7 Å. The figure is taken from [**barbry2015**].

the sub-nm regime [**barbry2015**]. This is demonstrated by considering 16 Å faceted NaNPs dimers in various configurations, shown in Figure 11. With flat surfaces aligned the conductance is maximised with a CTP and a fast blueshift seen as early as 5 Å. In contrast, with facet vertices aligned, a CTP only begins to emerge after contact between atoms. Screening in this arrangement is observed earlier at around 7 Å, likely due to charge only having to neutralise a small surface area. The facets demonstrate an atomic lightning rod effect that increases the field in the gap whilst minimising the conductance. All other configurations average to the expected result predicted using a spherical particle model. This demonstrates that experiments can in some sense become limited by surface roughness or even atomistic surface defects.

1.2.3 Limits of Critical Behaviour in Conductive Plasmonic Nanogaps

Both the blueshifting portion of the screening effect and CTP excitation require a conductance threshold to be surpassed in order for these effects to occur. Thresholds have been defined for a dimer containing a classical conductive linker, where the gap between particles of radius R has a width d, conductivity σ, and linker radius a [**perez2010**]. The formation of screened plasmons occurs at low conductances with a critical conductance for the dipolar bonding plasmon given by,

$$G_{\mathrm{SBDP}} = 2\varepsilon_0\omega_{\mathrm{BDP}}\frac{a^2}{d}, \quad \left(\sigma_{\mathrm{SBDP}} = \frac{2\varepsilon_0\omega_{\mathrm{BDP}}}{\pi}\right). \tag{7}$$

Reducing the conductance to a conductivity by removing a factor of $\pi a^2/d$ shows that screening is intrinsically independent of geometry and depends only on a critical conductivity. For larger contact widths or shorter

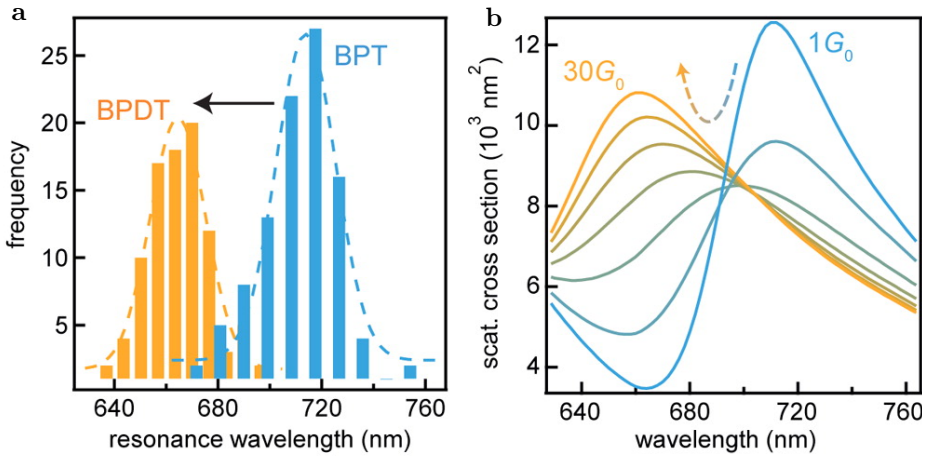

Figure 12: Experimental and theoretical scattering spectra of 80 nm AuNP on a planar Au mirror separated via variable conductance molecular spacer layer [benz2014]. Variable conductance molecular SAMs are formed from fractional mixing of BPT (insulating) and BPDT (conductance). The blueshift and attenuation of the coupled plasmon begins at $2G_0$ with the screened mode emerging once $G > 5G_0$.

linker lengths the conductance threshold increases to overcome the increased capacitive coupling. Experiments maintaining a fixed geometry whilst increasing the gap conductivity using fractional mixing of similar conductive and insulating SAMs have succeeded in showing a blueshift of coupled plasmons with an estimated $2G_0$ threshold [**benz2014**], as shown in Figure 12. A similar $2G_0$ threshold is also found in theoretically considered 1 nm dimer linkers [**perez2010**].

A second, much larger, threshold exists for CTP formation, occurring at,

$$G_{\mathrm{CTP}} = \varepsilon_0 \omega_{\mathrm{CTP}} \frac{R^2}{d}, \quad \left(\sigma_{\mathrm{CTP}} = \frac{\varepsilon_0 \omega_{\mathrm{CTP}}}{\pi} \left(\frac{R}{a} \right)^2 \right). \tag{8}$$

Unlike screening, CTP formation depends not only on the conductivity but also the junction geometry. The geometrical factor (R/a) represents the ratio between the total charge in the particle and the amount which can pass through a gap with fixed conductivity. Hence, a small, nanometre-scale but highly conductive junction between particles can accommodate sufficient current to maintain a CTP. This has been experimentally demonstrated in AuNP dimers separated by hollow spacer molecules and linked by a Au thread during exposure to high power laser pulses [**herrmann2014**, **tserkezis2014**].

Interestingly, qualitative agreement between QCM calculations and full quantum mechanical calculations suggest that the quantum nature of the system is of little importance. Even though the QCM uses a classical, resistive gap with conductances values characteristic of quantum transport, quantum effects on gap plasmons are accurately replicated. This implies that, despite the quantum nature of such small gaps, the effects on plasmon coupling only depend on the amount of charge transfer and not the mechanism by which it occurs. This links together work done using particle positioning [**savage2012**, **scholl2013**] with studies of interacting plasmonic system coupled with molecular linkers [**tan2014**, **cha2014**, **benz2014**]. Quantum tunnelling and quantised conductance still remains interesting cases, however, since both forms of conduction are unavoidable once gap sizes decrease below 0.5 nm. This is why the point at which the electric field is expelled from the gap is described as the quantum limit to plasmon confinement [**savage2012**]. For this reason, it is important to fully understand the relations between plasmonic hot spots and sites of (quantum) charge transfer.